We are IntechOpen,
the world's leading publisher of
Open Access books
Built by scientists, for scientists

6,900
Open access books available

186,000
International authors and editors

200M
Downloads

Our authors are among the

154
Countries delivered to

TOP 1%
most cited scientists

12.2%
Contributors from top 500 universities

CLARIVATE ANALYTICS
BOOK
CITATION
INDEX
INDEXED

WEB OF SCIENCE™

Selection of our books indexed in the Book Citation Index
in Web of Science™ Core Collection (BKCI)

Interested in publishing with us?
Contact book.department@intechopen.com

Numbers displayed above are based on latest data collected.
For more information visit www.intechopen.com

Geo Spatial Analysis for Tsunami Risk Mapping

Abu Bakar Sambah and Fusanori Miura

Abstract

Tsunami risk is a combination of the danger posed by tsunami hazard, the vulnerability of people to an event, and the probability of destructive tsunami. The spatial multicriteria approach made a possibility for integrating the vulnerability and risk parameters to assess the potential area that will be affected by the tsunami. The study applied the parameters of physical and social vulnerability and combined element at risk to assess tsunami risk in the coastal area of East Java Indonesia. All parameters in both tsunami vulnerability and tsunami risk assessment were analyzed through cell-based analysis in geographical information system. The weight of each parameter was calculated through the analytical hierarchy process. The results were provided as maps of tsunami vulnerability and tsunami risk. Tsunami risk map described five classes of risk. It described that coastal area with a low elevation and almost flat identified as high risk to the tsunami. The coastal area with a high density of vegetation (mangrove) was defined as the area with low level of tsunami risk. The existence of river and other water canals in coastal area was also analyzed for generating tsunami risk map. Risk map highlights the coastal areas with a strong need for tsunami mitigation plan.

Keywords: tsunami, vulnerability, risk, geospatial, weighted overlay, GIS

1. Introduction

Tsunami can be defined as a series of waves created by an impulsive disturbance in the water body. It causes severe damage to coastal areas. A tsunami wave could be less than 1 m high in the open ocean and traveling at up to 800 km/h in which the wave energy will be extended from the surface to the ocean floor. The wave energy of tsunami will be compressed into a much shorter distance when it approaches the coast, creating potentially large destructive to the coastal areas [1]. A tsunami can be generated when the sea floor abruptly deforms and a bottom layer of water body displaces the overlying water vertically. One kind of earthquake that is related to the crustal deformation of the earth is tectonic earthquakes. When these earthquakes happen in the bottom of the sea, the water layer above the deformed area is displaced from its equilibrium position. Waves are formed as the displaced water mass, which occurs due to the impact of gravity. A tsunami can be generated when large areas of the sea floor subside.

In the deep water of the open ocean, the speed of tsunami waves can be up to 800 km/h. The energy wave of tsunami will decrease dramatically when it approaches the coast, but its height can be 10 times or more and have catastrophic consequences to the coastal areas. As a result, the low-lying areas of the coast and the areas near

bay mouths or tidal flats will be highly vulnerable to the tsunamis. A tsunami can be generated through four special events, which are illustrated in **Figure 1**. These figures described that the distribution of tsunami was based on the effect and magnitude, which describes that mostly this event occurred in the area of "ring of fire," a zone of active earthquakes and volcanoes, surrounds much of the Pacific Ocean.

1. Subduction zone

One of the many plates that make up earth's outer shell descends under an adjacent plate. This kind of boundary is called a subduction zone. When the plates move suddenly in an area where they usually stick, an earthquake will happen.

2. Between earthquakes

Stuck to the subducting plate, the overriding plate gets squeezed. Its leading edge is dragged down, while an area behind bulges upward. This movement goes on for decades or centuries, slowly building up stress.

3. During earthquakes

An earthquake along a subduction zone happens when the leading edge of the overriding plate breaks free and springs seaward, raising the seafloor and water above it. This uplift starts a tsunami. Meanwhile, the bulge behind the leading lead collapses, flexing the plate downward and lowering the coastal area.

4. After earthquakes

Part of the tsunami races toward nearby land, growing taller as it comes into shore. Another part heads across the ocean toward distant shores.

The 2004 Indian Ocean earthquake and tsunami, the 2011 Tohoku earthquake and tsunami, and the 2018 Sulawesi Indonesia earthquake and tsunami show that
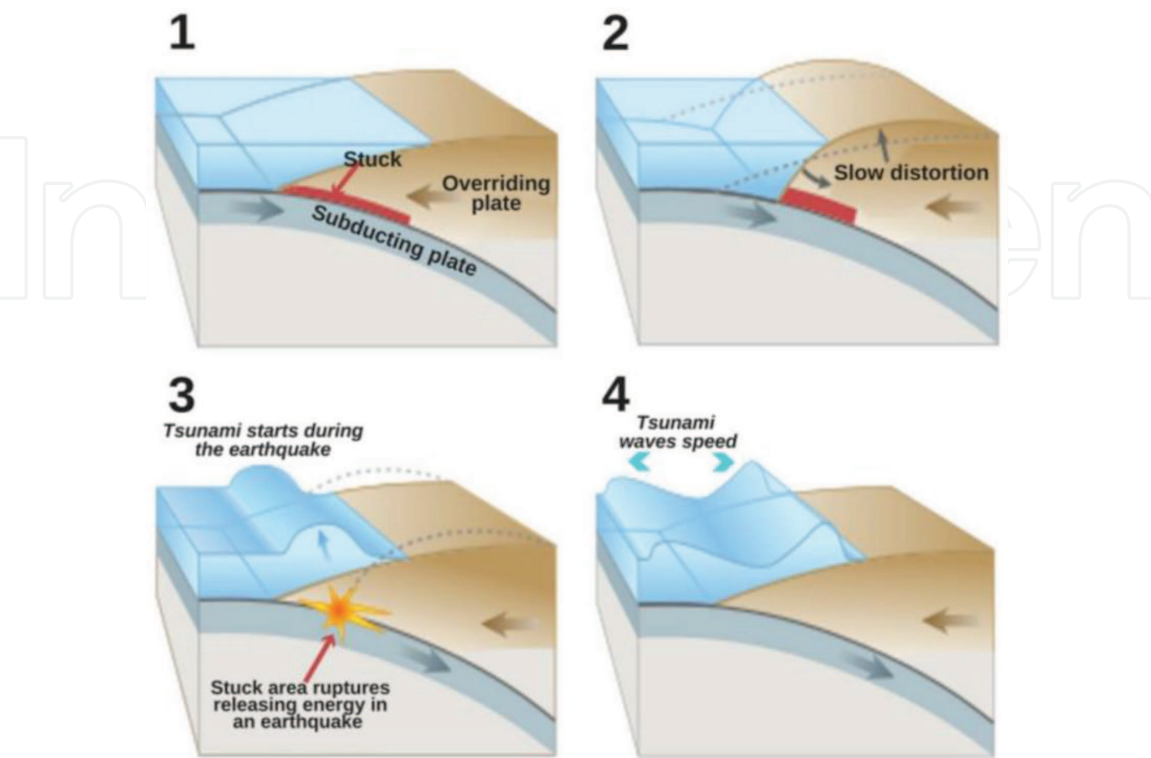

Figure 1.
Tsunami generations [2].

this natural disaster is almost periodical event in 7–10 years along the area of ring of fire, a major area in the basin of the Pacific Ocean where many earthquakes and volcanic eruptions occur. The natural disaster includes tsunami is the even that it is impossible to reduce its occurrence, but the impact can be minimized by performing an initial assessment related to vulnerability and risk mapping.

Tsunami risk mapping combines the results of the tsunami vulnerability and tsunami hazard. This illustration is described in **Figure 2**. Assessing tsunami vulnerability and risk can provide important information for tsunami mitigation plan. This also plays an important role in preparing and mitigating for the future events of tsunami [3, 4]. A risk of a tsunami disaster is defined as the mathematical product of tsunami vulnerability and tsunami hazard. It refers to the expected loss from a given hazard to a given element at risk [5]. A disaster is a function of the risk process. Risk results from the combination of hazards, vulnerability, and insufficient capacity to minimize the negative impact of risk. In general, risk assessment combines the results of the hazard and vulnerability assessments [6].

Moreover, disaster risk assessment is a qualitative or quantitative approach to determine the nature and extent of disaster risk by analyzing potential hazards and evaluating existing conditions of exposure and vulnerability that together could harm people, property, services, livelihoods, and the environment on which they depend [7].

The implementation of tsunami risk assessment includes the effectiveness of mitigation will be the practical outcome of the study. Risk map can be used for both tsunami evacuation route and tsunami evacuation building setting. In order to create tsunami risk map, it is necessary for assessing the vulnerability areas due to tsunami in which the physical and social parameters of vulnerability are needed.
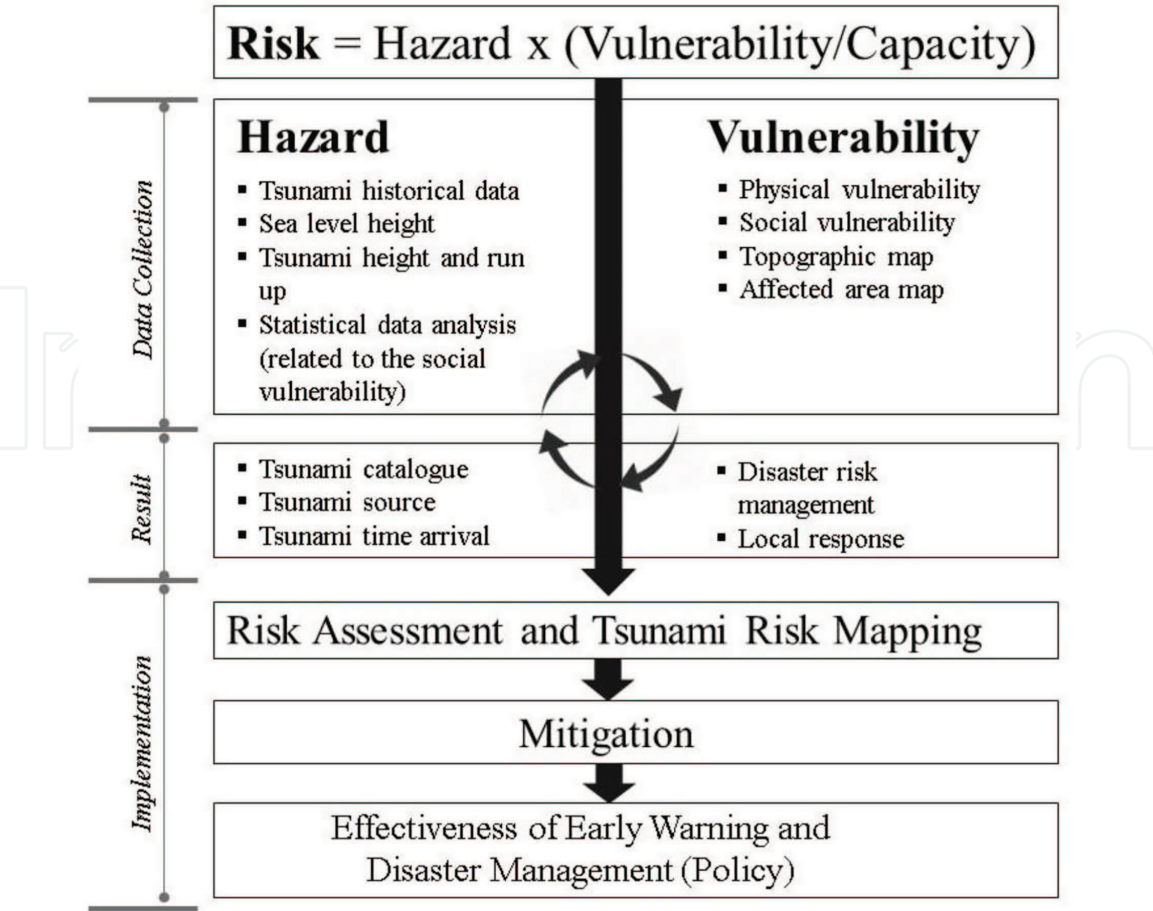

Figure 2.
General concept of the study.

Many approaches have been applied in order to map the potential areas affected by tsunami. A novel approach of tsunami vulnerability mapping in the application of geographical information system (GIS) together with the analysis of satellite remote sensing has been done to assess the risk areas due to tsunami. An overview of the use of geospatial data with emphasis on satellite remote sensing data and of the approaches used for hazard assessment is given. Satellite images have the advantage of being able to deliver simultaneous images of wide areas [8–11]. Remote sensing imagery is already used for hazard-related applications since the advent of research-oriented satellite systems and sensors four decades ago.

In addition, with the aid of the GIS, geospatial analysis helps prioritize the decision-making process using georeference data. Geospatial analysis through the application of spatial multicriteria analysis is vastly different from conventional multicriteria decision-making techniques, due to the inclusion of an explicit geographic element. Spatial multicriteria analysis uses information on both the criterion values and the geographical information, in addition to the decision-maker's preferences with respect to a set of evaluation parameters [12, 13].

Some of the previous studies on tsunami vulnerability have analyzed remote sensing data, primarily to assess the physical vulnerability and risk of coastal areas. In addition to such studies, the application of remote sensing in hazard and vulnerability assessment related to ecological and socioeconomic vulnerability has been analyzed. Previous studies have also applied moderate-resolution optical satellite images and integrated analysis using GIS to identify inundation areas due to tsunamis [14–17]. GIS mapping of tsunami vulnerability has also applied using the Shuttle Radar Topography Mission (SRTM) to obtain the topographic data of the study area [18]. Another spatial analysis method has applied soil type, urban form, and social type system for the potential natural hazard mapping [Hsien] and has determined the tsunami-vulnerable area by comparing building damage map with the topography data, which is discussed with regard to land elevation, land use, and the distance from the coast [19].

Mapping of the 2011 Tohoku Earthquake tsunami inundation and run-up by survey also has been published [20]. A novel approach from the Coastal Risk Analysis for Tsunamis and Environmental Remediation (CRATER) project was applied for assessing tsunami vulnerability on a regional scale using ASTER imagery and SRTM version 3. This work analyzed the vulnerability of coastal zones and inland areas using the parameters of infrastructural, geomorphological, and ecological features for coastal zones, and parameters of land use, altimetry, and distance from the shoreline for inland areas [21]. Tsunami vulnerability mapping along coastal area of East Java also applied using high resolution of elevation data from NEXTMap World 10.

The main contribution of this book chapter is to utilize the remote sensing technology based on geospatial technique to investigate the spatial tsunami risk impact on coastal zones. In this regard, the main objective is to establish a geospatial tool for monitoring the tsunami risk impacts along the coastal area of East Java, Indonesia.

2. Method

2.1 Study area

The study was applied at the south coastal area of East Java, Indonesia (**Figure** 3). The coastal areas of East Java including Malang district and Jember district were known as one of the important marine fishery resource spots in East Java. These areas
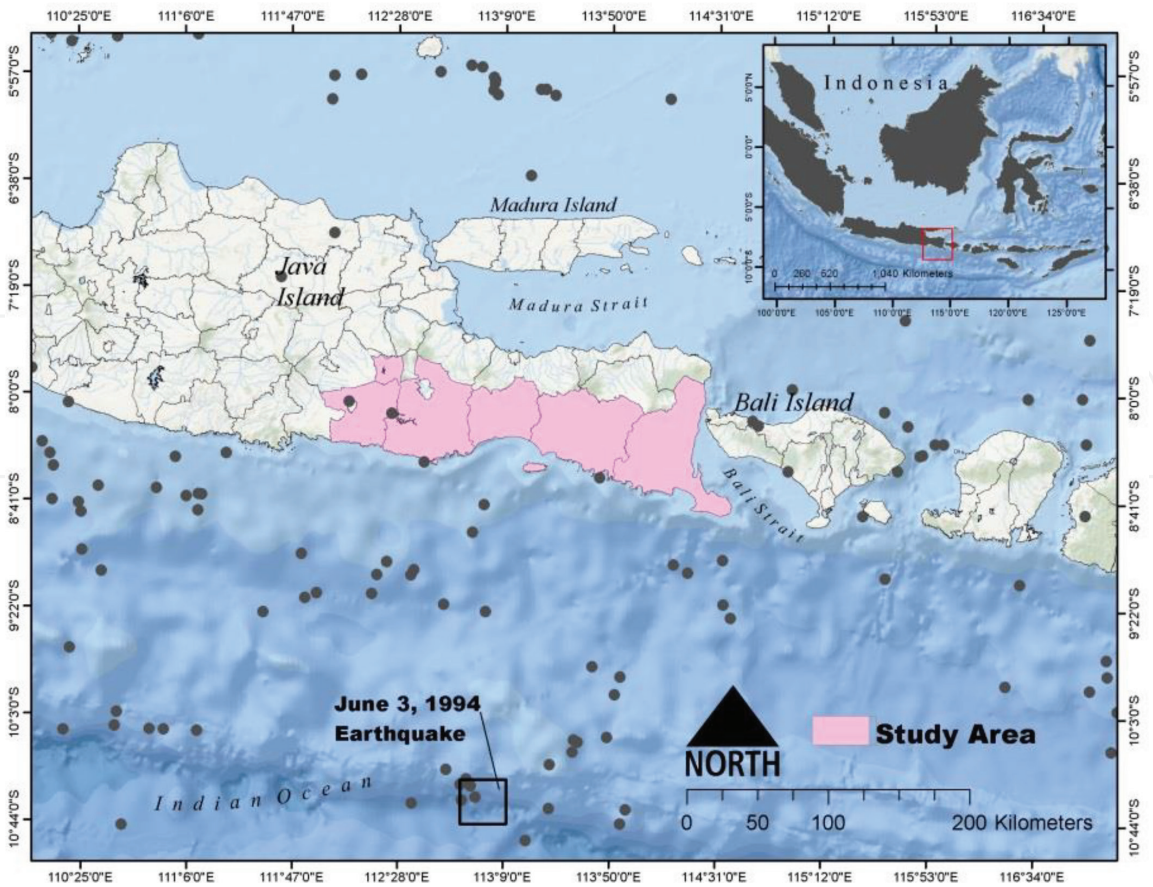
Figure 3.
Study area was the coastal area of East Java. [Points represent historical data of earth quake epicenter].

also affected by 1994 tsunami event along the coastal area of East Java. The tsunami genic earthquake occurred on June 3, 1994, in the Indian Ocean about 200 km south of Java. The earthquake, which had a surface-wave magnitude of 7.2 and a moment magnitude of 7.8 at 10.51°S and 112.87°E, generated a devastating tsunami that took the lives of more than 200 East Java coastal residents; with maximum run-up value of 9.50 m measured at Rajekwesi area, east part of the study area [22, 23].

2.2 Dataset

Tsunami vulnerability map was created using two deference sources of elevation data. Digital Elevation Model (DEM) from the ASTER Global Digital Elevation Model (ASTER GDEM) version 2 was applied to generate elevation and slope map. The Advanced Spaceborne Thermal Emission and Reflection Radiometer (ASTER) GDEM is a joint product developed and made available to the public by the Ministry of Economy, Trade, and Industry (METI) of Japan and the United States National Aeronautics and Space Administration (NASA).

DEM of NEXTMap World 10 also applied for creating the elevation and slope parameter as a digital elevation data for physical tsunami vulnerability mapping. NEXTMap World 10 provides a 10 m resolution and makes the wide possibility for elevation analysis in large areas. This DEM was the combination process from SRTM90 v2.1: 90 m Digital Surface Model (DSM) collected from Interferometric Synthetic Aperture Radar (IFSAR) in February 2000, SRTM30: 30 m DSM also collected from IFSAR in February 2000, ASTER 30v2.0: 30 m DSM collected from optical sensor from 2005 to 2011, ICESat as a point data of LiDAR from Geoscience Laser Altimeter System (GLAS) satellite collected from 2003 to 2010, and GTOPO30: 30 m DSM collected from eight raster and vector data from USGS in 1996.

In order to map the land use of the study area, ALOS satellite imagery with the instrument of the Advanced Visible and Near Infrared Radiometer type 2 (AVNIR-2) with the spatial resolution of 10 m was analyzed. Landsat 8 Operational Land Imager (OLI) with the spatial resolution of 30 m also applied for this land use map. Moreover, seismic data of the study area from 1992 to 2014 collected from the United States Geological Survey (USGS), and downloaded from http://earthquake. usgs.gov/earthquakes/search/ was used as a supporting parameter for tsunami vulnerability in which further will generate the seismic map. In order to apply the overlay process, vector base map of East Java Indonesia was used to prepare vector data of coastal morphology, coastal line (coastal proximity), and river proximity.

2.3 Satellite image processing for land cover classification

2.3.1 Digital number to radiance conversion

The algorithm that applied for the conversion of DN to radiance applied Eq. (1) [24].

$$L_\lambda = G_{rescale} \times QCAL + B_{rescale} \tag{1}$$

in which L_λ is the spectral radiance at the sensor's aperture (W/m^2/sr/μm), $G_{rescale}$ is the rescaled gain, $QCAL$ is the digital number (DN), and $B_{rescale}$ is the rescaled bias. **Table** 1 described rescaled gains and biases for ALOS AAVNIR-2 satellite.

2.3.2 Radiance to reflectance conversion

The conversion of radiance to reflectance applied the algorithm of Eq. (2) [25].

$$\rho_\lambda = \pi \times L_\lambda \times d^2/ESUN_\lambda \times \cos\theta_s \tag{2}$$

where ρ_λ is the unitless planetary reflectance, L_λ is the spectral radiance at the sensor's aperture, d^2 is the earth-sun distance in astronomical units from a nautical handbook, $ESUN_\lambda$ is the mean solar exoatmospheric irradiance, and θ_s is the solar zenith angle in degree.

2.3.3 Decision tree classification

Satellite image classification was applied a decision tree classification. The value that was used for the range of classification was based on the normalized difference vegetation index (NDVI) value. NDVI is a measure of the difference in reflectance between these wavelength ranges with the values from −1 to 1. NDVI value more than 0.5 indicates dense vegetation and the value less than 0 indicates no vegetation including water. NDVI was calculated using Eq. (3) [26].

Band	$G_{rescale}$	$B_{rescale}$
1	0.5888	0
2	0.5730	0
3	0.5020	0
4	0.8350	0

Table 1.
Rescaling gains and biases used for DN to spectral radiance conversion (for ALOS AVNIR-2).

$$NDVI = \frac{(NIR - VIS)}{(NIR + VIS)} \tag{3}$$

NIR is the reflectance of near-infrared band and *VIS* is that of visible red band of satellite sensor. Band 3 is represented in red and band 4 is *NIR*.

Decision tree classification is a flowchart like a tree structure where each internal node donates a test on an attribute and each branch represents an outcome of the test and leaf nodes represent the class distribution [27]. The concept of decision tree classification is illustrated in **Figure** 4. The NDVI value was applied as a basic expression. Each decision is based on a numerical comparison with a selected threshold index, which makes the whole process easily repeatable. The decision tree is also applied in the study of tsunami vulnerability using ASTER imagery [21]. The main advantage of such approach is that data from many different sources can be processed together to make a single decision tree classifier. Decision tree tool is nonparametric; therefore, it makes no assumption on the distribution of the input data [28]. The NDVI represents a simple numerical indicator that can be used in analyzing remote sensing imagery and assessing whether the target being observed contains live green vegetation.

Decision tree classification step applied as below.

1. Entering the rules

   a. The decision tree tool starts with one empty decision node that will divide the pixels in the dataset into two groups using binary decision expression entered into that empty node.

   b. The first decision will be based on the medium resolution of satellite image. The decision can be created by adding the decision node labeled.

   c. Expression of the decision can be set in the decision node based on the criteria of analysis (for example, NIR < 0.09). The text will appear in the decision node in the graphical view of decision tree.

   d. The variable pairings dialog appears after adding the expression.

2. Pairing the expression variable with a file

In this step, an expression that already set will be linked to the associate file. This describes the decision tree that when evaluating this decision expression, the expression should be calculated from the associate file.

2.4 Data processing and analysis by modeling tsunami physical, social, and risk vulnerability

2.4.1 Physical and social vulnerability

Vulnerability mapping has been generated using the parameter of elevation, slope, coastal proximity, river proximity, coastal morphology (illustrated coastal type), and land use. Together with hazard or capacity, tsunami vulnerability is one of the parameters in assessing tsunami risk. The cell-based analysis was applied in combining all parameters through GIS process. Each tsunami vulnerability parameter was classified into five classes for vulnerability based on the criteria range as shown in **Tables 1** and **2**. The coastal proximity classes in meter were calculated
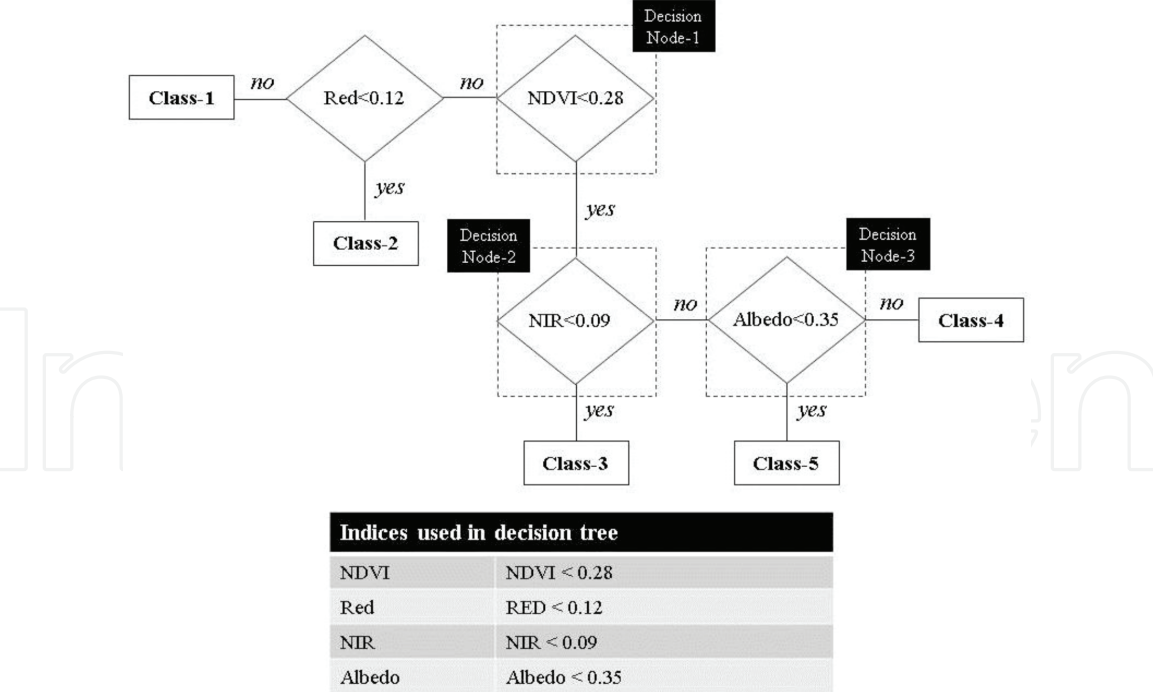
Figure 4.
Illustration of decision tree applied in satellite image classification.

based on the measured run-up and water height in the surveyed area during the last tsunami event in the coastal area of East Java on June 3, 1994. It was calculated using algorithm Eq. (4) [29, 30].

$$\log X_{max} = \log 1400 + \tfrac{4}{3} \log (Y_0/10) \qquad (4)$$

X_{max} is the maximum reach of the tsunami over land, and Y_0 is the height of the tsunami at the coast.

Moreover, land use map was generated from supervised classification process of satellite mage. Maximum likelihood methods were applied in the supervised process. Land use class was divided into five classes, and each class was reclassified based on the vulnerability classes as shown in **Tables 2** and **3**. The selected sample for each land use class in the reflectance value of satellite digital image was collected to calculate the accuracy of classification result. The classification of land use was based on the spectral signature defined in the training set.

Vulnerability class	Physical vulnerability		
	Elevation (m)[1]	Slope (%)[2]	Land use[3]
High	<5	0–2	Urban
Slightly high	5–10	2–6	Agriculture
Moderate	10–15	6–13	Bare soil
Slightly low	15–20	13–20	Water
Low	>20	>20	Forest

[1]*Ref. [31].*

[2]*Ref. [32].*
[3]*Ref. [30].*

Table 2.
Physical tsunami vulnerability value range (1).

Vulnerability class	Physical vulnerability		
	Coastal distance (m)[1]	River proximity (m)[2]	Coastal type[2]
High	<293	0–100	V bay
Slightly high	293–514	100–200	U bay
Moderate	514–762	200–300	Cape
Slightly low	762–1032	300–500	Straight
Low	>1032	>500	Neutral

[1]Based on Eq. (4) calculations.
[2]Ref. [33].

Table 3.
Physical tsunami vulnerability value range (2).

In the term of social vulnerability analysis, a social parameter was needed. Social vulnerability can be defined as the exposure of groups or individuals to unexpected changes and disruption to livelihoods [34]. Social vulnerability also can be measured as a result of social and place inequalities [35]. Social vulnerability is defined also as the limitation of a community to the impact of natural disasters that influence its ability or resilience in order to mitigate and recover from and prepare for the impacts of disaster [36]. Social vulnerability map was created using four parameters and weighted equally based on the criteria as explained in **Table 4**.

2.4.2 Spatial multicriteria analysis

The parameters of both physical and social vulnerabilities are displayed in grid cells, which are then classified based on their value to five classes of vulnerabilities; they represent low, slightly low, medium, slightly high, and high vulnerability. All parameters will be overlaid in the raster data format (cell-based) based on their weight. Weighted overlay describes the technique for applying a common measurement scale of values to diverse and dissimilar inputs to create an integrated analysis. Weighted overlay also describes the type of suitability analysis that helps in analyzing site conditions based on multiple criteria. By identifying areas based on their criteria, weighted overlay analysis allows the user to combine weight and rank several different types of information and give the visualization of the result, in which multiple parameters can be evaluated at once [38]. Weights for all parameters are constructed in terms of pair-wise comparison matrix through analytical hierarchy process (AHP).

AHP can be defined as an approach for organizing and analyzing complex decisions, based on mathematics (matrix calculation) and psychology. In this study, AHP helps in constructing the weight of each parameter by applying expert judgment. The result from AHP calculation then overlaid spatially in GIS methods. The concept of pair-wise comparison and AHP calculation is illustrated in four steps below.

Step 1. Construct pair-wise comparison matrix, in which each parameter will be compared to others as described below.

	c1	c2	c3	c4	c5
c1	1	c_1/c_2	c_1/c_3	c_1/c_4	c_1/c_5
c2	c_2/c_1	1	c_2/c_3	c_2/c_4	c_2/c_5
c3	c_3/c_1	c_3/c_2	1	c_3/c_4	c_3/c_5

c4	c_4/c_1	c_4/c_2	c_4/c_3	1	c_4/c_5
c5	c_5/c_1	c_5/c_2	c_5/c_3	c_5/c_4	1
sum	S_1	S_2	S_3	S_4	S_5

c1: parameter 1   c4: parameter 4
c2: parameter 2   c2: parameter 5
c3: parameter 3

Step 2. Normalized matrix

$$\begin{bmatrix} (c1/c1)/s1 & (c1/c2)/s1 & (c1/c3)/s3 & .. & (c1/c5)/s5 \\ (c2/c1)/s1 & (c2/c2)/s1 & (c2/c3)/s3 & .. & (c2/c5)/s5 \\ (c3/c1)/s1 & (c3/c2)/s1 & (c3/c3)/s3 & .. & (c3/c5)/s5 \\ .... & .... & .... & .. & .... \\ (c5/c1)/s1 & (c5/c2)/s1 & (c5/c3)/s3 & .. & (c5/c5)/s5 \end{bmatrix} \rightarrow \begin{bmatrix} s1.1 \\ s1.2 \\ s1.3 \\ ...... \\ s1.5 \end{bmatrix} \begin{bmatrix} n1 \\ n2 \\ n3 \\ ... \\ n5 \end{bmatrix}$$

n5: fifth iteration of principal eigenvalue

Step 3. Calculation of consistency ratio

$$CR = \frac{CI}{RI} \tag{5}$$

$$CI = \frac{(\lambda_{max} - N)}{(N - 1)} \tag{6}$$

in which, CR is consistency ratio, CI is consistency index, RI is random consistency index, λ_{max} is the principal eigenvalue, N is the number of the comparison matrix.

RI values depend on matrix size (N) as explained below.

Matrix size (N)	1	2	3	4	5	6	7	8	9	10
RI	0	0	0.58	0.90	1.12	1.24	1.32	1.41	1.45	1.49

If the value of CR in less than or equal to 0.10 (10%), the inconsistency is acceptable. If the CR is more than 10%, then the subjective judgment needs to be revised.

In AHP processing, pair-wise matrix was done to compare the importance of each parameter using Saaty's nine scales. In the second step of AHP, the normalized matrix was applied to calculate the eigenvalue of the parameter in which the parameter's weight was constructed. Eigenvalue represents the weight of each parameter, and it is applied after the fifth iteration of principal eigenvalue. Consistency ratio (CR)

Parameters (a)	∑ (b)	Proportion* (c)	Score** (d)
Population density	P	(b)/total population	(c)/maximum proportion
Gender	G	(b)/total woman	(c)/maximum proportion
Age***	A	(b)/total age	(c)/maximum proportion
Disabilities	D	(b)/total disabilities	(c)/maximum proportion

Determine the factor of each village divided by number per subdistrict.

**The same value for all places on all the social variables.*
***Number of elderly and children.*

Table 4.
Social vulnerability parameter [37].

calculation was done to determine the inconsistency from AHP process in which RC should be less than 10%. Weighted linear combination is very straightforward in a raster GIS, and factors are combined by applying a weight value to each followed by a summation of the results to create both physical and social vulnerabilities using Eq. (7) [36] and Eq. (8).

$$\text{Vulnerability} = \sum (W_i \cdot X_i) \tag{7}$$

$$\text{Total vulnerability} = \sum (\text{physical vulnerability} \times \text{weight}) \\ + (\text{social vulnerability} \times \text{weight}) \tag{8}$$

where W_i is the weight value of the parameter i and X_i is the potential rating of the factor.

The illustration of weighted/cell-based overlay is described in **Figure 5**.

2.4.3 Risk assessment

Risk combines the vulnerability result with the probable level of loss to be expected from a predictable magnitude of hazard (which can be considered as the manifestation of the means that produces the loss). Risk, vulnerability, and hazard are the three factors or elements, which we are considering here in this pseudoequation. The terminology of risk also given by factor analysis of information risk which may be related to disaster is "the probable frequency and probable magnitude of
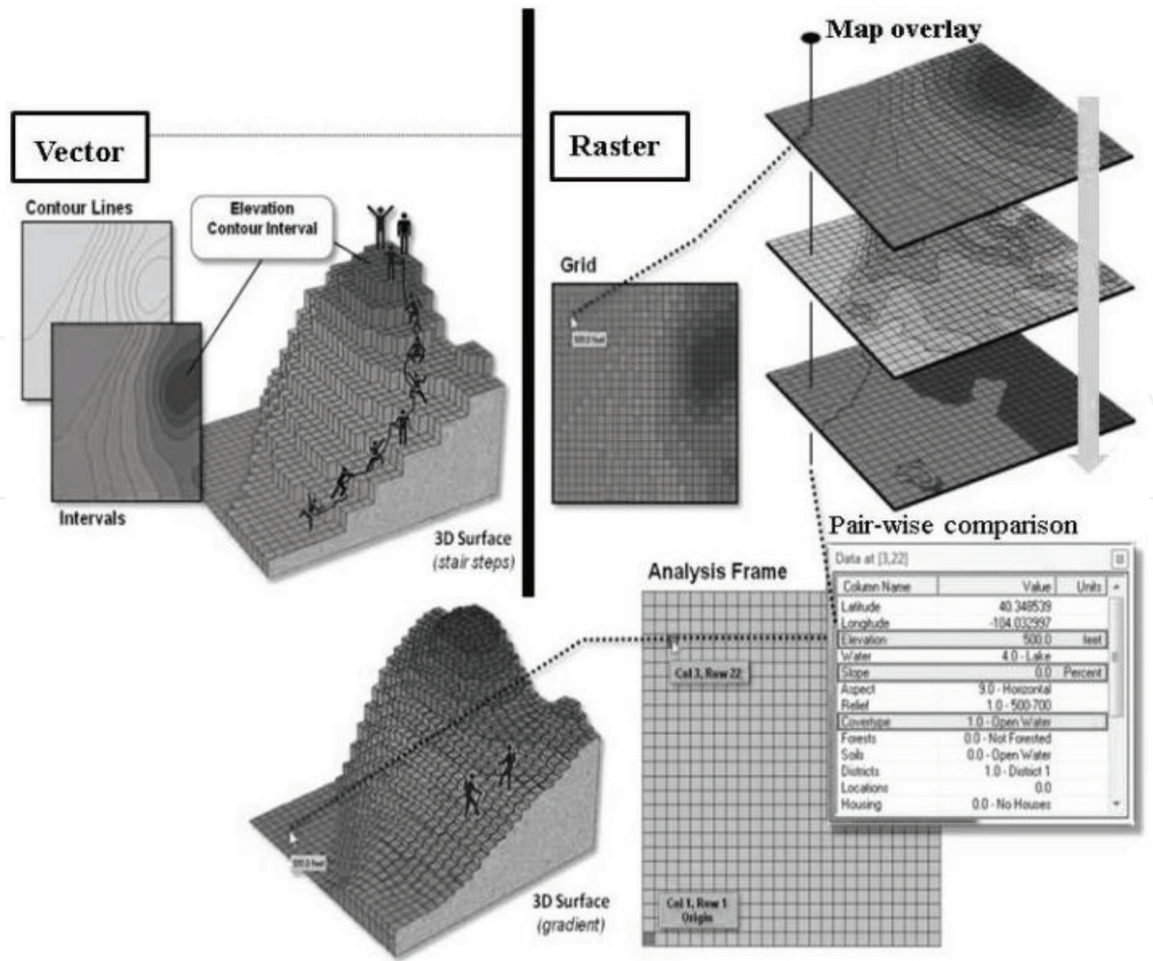

Figure 5.
Weighted/cell-based overlay illustration.

predicted losses" [34]. The value of risk can be calculated as the product of vulnerability and hazard level. Vulnerability level ranges from 1 to 5 from low to high vulnerability and hazard level ranges from 1 to 4. Risk was calculated using Eq. (9).

$$R = V \times H/4 \tag{9}$$

in which R is a risk, V is vulnerability, and H is a hazard.

R must be an integer number ranging from 1 to 5, where 5 stands for the maximum risk level. Once risk level has been calculated, it will be possible to plot it on a risk map by the process of GIS. Risk map was also generated using weighted cell-based overlay. Weighted overlay analysis allows the user to combine weight and rank several different types of information and visualize it, so multiple factors can be evaluated at once [38].

3. Result and discussion

3.1 Image classification for land use mapping

Land use is one of the parameters that is applied in the spatial multicriteria analysis in creating physical tsunami vulnerability map. Land use map was created using decision tree classification in which the concept was as illustrated in **Figure 4**. The result of the image classification is described in **Figure 6**.

In order to create a tsunami vulnerability map based on the land use, a category of vulnerability classes was applied in the land use raster map. Tsunami vulnerability map was created using the criteria as described in **Table 1**, in which it briefly described
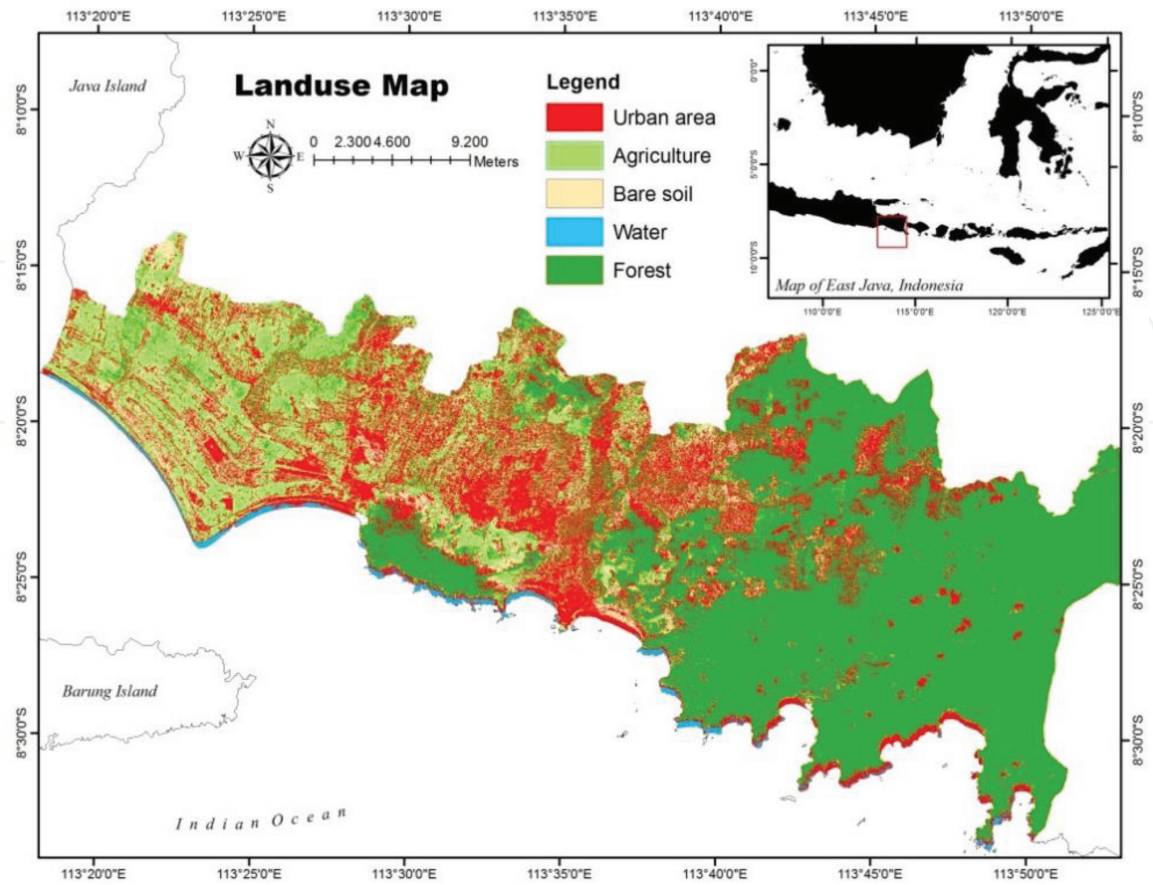

Figure 6.
Land use of the study area as the result of satellite image processing.

that high class of vulnerability was set for the land use of urban area, slightly high for the agriculture, moderate for the bare soil area, slightly low for the water body, and low vulnerability class for the forest area. The reclassification of land use based on those criteria created the tsunami vulnerability map as shown in **Figure 7**.

Mostly, urban area was spread in the western part along the coastal of study area. These areas are known as a center of fishery activities with many fishing bases. An urban area spread in the low elevation until flat area, and it will get serious impact when tsunami wave approaches the coastal area. In the area with high density of coastal vegetation, the damage impact of the tsunami will be lower. Coastal vegetation, such as mangrove, can act as the barrier zone to reduce the energy of tsunami wave when it hits the coastal area, and it will also minimize the impact of tsunami.

3.2 Tsunami vulnerability mapping

Physical vulnerability map was created using six criteria with different weight. The weight of each criterion was calculated using pair-wise comparison matrix in the AHP approach. Some experts in the theme of tsunami prevention system and management were collected to construct the matrix of criteria. Pair-wise comparison matrix and the result calculation of CR for the physical vulnerability are described in **Table 5**.

Moreover, social vulnerability was calculated based on social database in the theme of population density, gender, age, and also education level. The map of these criteria is based on scoring and weight of each criterion, which will be basic information in determining both evacuation route and evacuation building. The calculation was based on [39] in which the first step in calculation was calculation of X for determining the percentage of woman. This calculation was using Eq. (10).
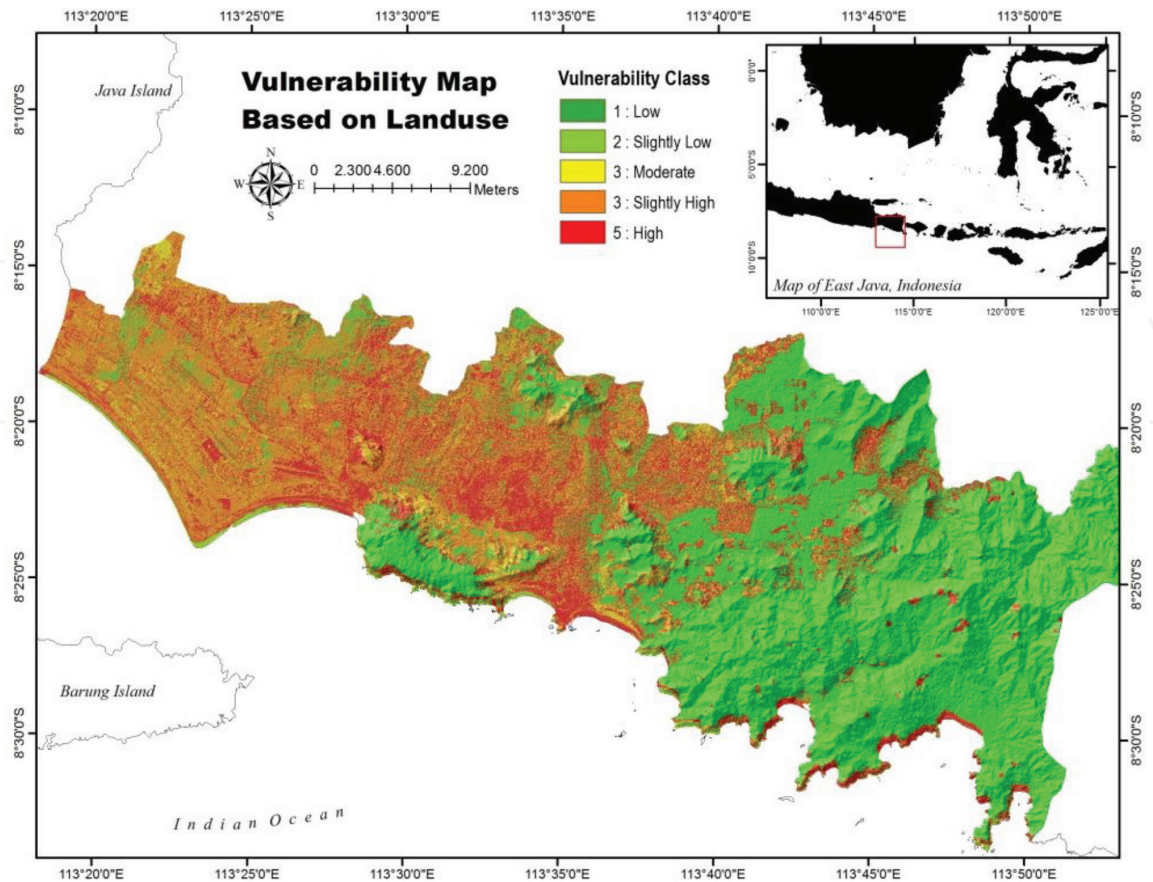

Figure 7.
Tsunami vulnerability map based on land use.

The second step was to calculate the score of woman by calculating the ratio of X for determining scale using Eq. (11)

$$X = \frac{\text{total of woman in district}}{\text{total of woman in study area}} \tag{10}$$

$$\text{score for woman} = \frac{X}{\text{maximum X}} \tag{11}$$

Scoring of the parameter was calculated using **Table 6**.

By using Eq. (8), tsunami vulnerability map was created. The map of tsunami vulnerability is shown in **Figure 8**, which illustrated that from the analysis of both physical and social parameters of vulnerability, the high class of tsunami vulnerability area is found in the area with low elevation along the coastal area. The coastal area vulnerable to tsunami inundation, the urban area, and infrastructure are not uniformly at risk within the flood zone [35]. The affected area due to tsunami is related both to vulnerability and to the tsunami wave energy; it is also related to the source of earthquake epicenter. Damage level to buildings in the urban area depends on building type and the height of the building and on inundation depth [37] or could depend on vegetation density around the coastal area. Mangrove can be a buffer zone for the impact of tsunami wave and it is assumed that it will reduce tsunami impact.

3.3 Seismic analysis and tsunami run-up

Seismic data consist of physical measurements, seismic sources, seismic waves, and their propagating media. The purpose of seismic data processing is to learn something about the earth's interior. It needs to figure out some specific relations between the intended targets and measurable parameters in order to understand certain aspects of the earth [38]. All initial tsunami warnings are based on early detection and characterization of seismic activity. Due to the fundamental differences in nature between the solid earth in which an earthquake takes place and the fluid of ocean where tsunami gravity waves propagate, the vast majority of earthquakes occurring on a daily basis do not trigger appreciable or even measurable tsunamis. It takes a large event (magnitude more than 7.0) to generate a damaging tsunami in the near field and a great earthquake (magnitude more than 8.0) to generate a tsunami in the far field [39].

	Normalized principal eigenvector (fifth iteration)						
	c.1	c.2	c.3	c.4	c.5	c.6	%
c.1	0.28	0.29	0.353	0.288	0.184	0.273	28
c.2	0.187	0.194	0.176	0.231	0.184	0.182	19
c.3	0.14	0.194	0.176	0.231	0.245	0.136	18
c.4	0.112	0.097	0.088	0.115	0.184	0.182	12
c.5	0.187	0.129	0.088	0.077	0.122	0.136	13
c.6	0.093	0.097	0.118	0.058	0.082	0.091	9

CI = 0.032, CR = 2.6%.
c.1: elevation; c.2: slope; c.3: coastal distance; c.4: river proximity; c.5: coastal type; c.6: land use.

Table 5.
Pair-wise comparison matrix.

Parameter (a)	Proportion (b)	Score (c)	Weight (d)
Population density	(b)/total population	(c)/maximum proportion	25
Gender	(b)/total woman	(c)/maximum proportion	25
Age	(b)/total age	(c)/maximum proportion	25
Disabilities	(b)/total disabilities	(c)/maximum proportion	25

Table 6.
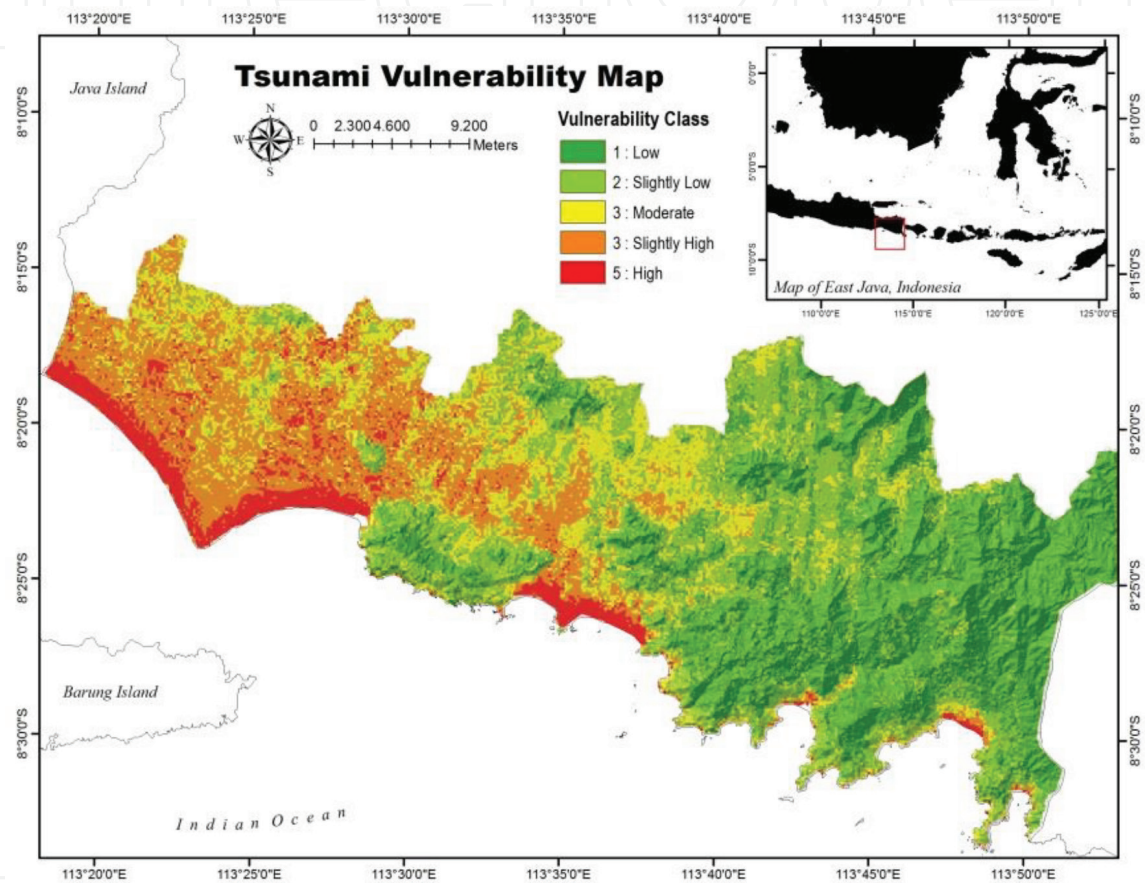*Weight of the parameter for social vulnerability [39].*

Figure 8.
Tsunami vulnerability map.

Coastal area of East Java was identified as the area with high number of the seismic point with the depth of 1–5 km in average and the range of magnitude was 1 to more than 6. As the result, the coastal area of East Java can be classified as a high risk to tsunami. Based on historical event, it was a magnitude of 7.8 Mw in the depth of 18 km that identified the geographic position in latitude of −10.477° and longitude of 112.835°, caused a big tsunami, and affected the coastal area of East Java.

Tsunami run-up parameter plays as an important role in determining tsunami risk. This parameter is also classified as a main parameter in hazard criteria. The historical tsunami event close the coastal area of East Java in 1994 was used as basic data for run-up analysis. The maximum run-up was recorded around 11.2 m at Tempurejo district, and minimum run-up was 3.1 m in the area of Puger district. The run-up analysis described seven run-up points along the coastal area. The last survey described that in the North West part of the study area (Cape Pelindu), a small fishermen village where a fishery created a sort of barrier to the sea water,

separating houses from the ocean [37]. The fishery defense wall and three typical straw houses were destroyed. According to eyewitnesses, three big waves followed each other, the third one being the biggest. The measured maximum water height was 3.20 m, and the maximum water ingression was about 350 m.

3.4 Tsunami risk mapping

Tsunami risk map describes five classes of risk level. Moderate until the high class of tsunami risk was found in the western part of the study area. This area is mostly covered by flat elevation, bare soil, and the area that contains rare density of coastal vegetation and high density of building area. Previous tsunami event recorded that run-up of 4.85–5.85 m happened in this area.

Tsunami risk map was created by the spatial integration of vulnerability and hazard map. Tsunami risk can be defined as a combination of the danger posted by tsunami event, the vulnerability of people to tsunami hazard, and the probability of destructive *tsunami*. Tsunami risk as the result of this study is described in **Figure 9**. Tsunami waves may undergo extensive refraction and create a process that may converge their energy to particular areas on the coastal area and increase the heights and run-up of the waves when they hit the coastal area. High risk of a tsunami is depending on the depth of water, the coastal geomorphology, the direction of the tsunami wave, and the existence of rivers or other water canals.

The high density of mangrove in coastal areas and the existence of reefs can play as a barrier to reduce the effect of the tsunami wave, as well as the islands with steep-sided fringing are only at moderate risk from tsunamis. Study about predicting tsunami inundation area using coastal vegetation density was carried
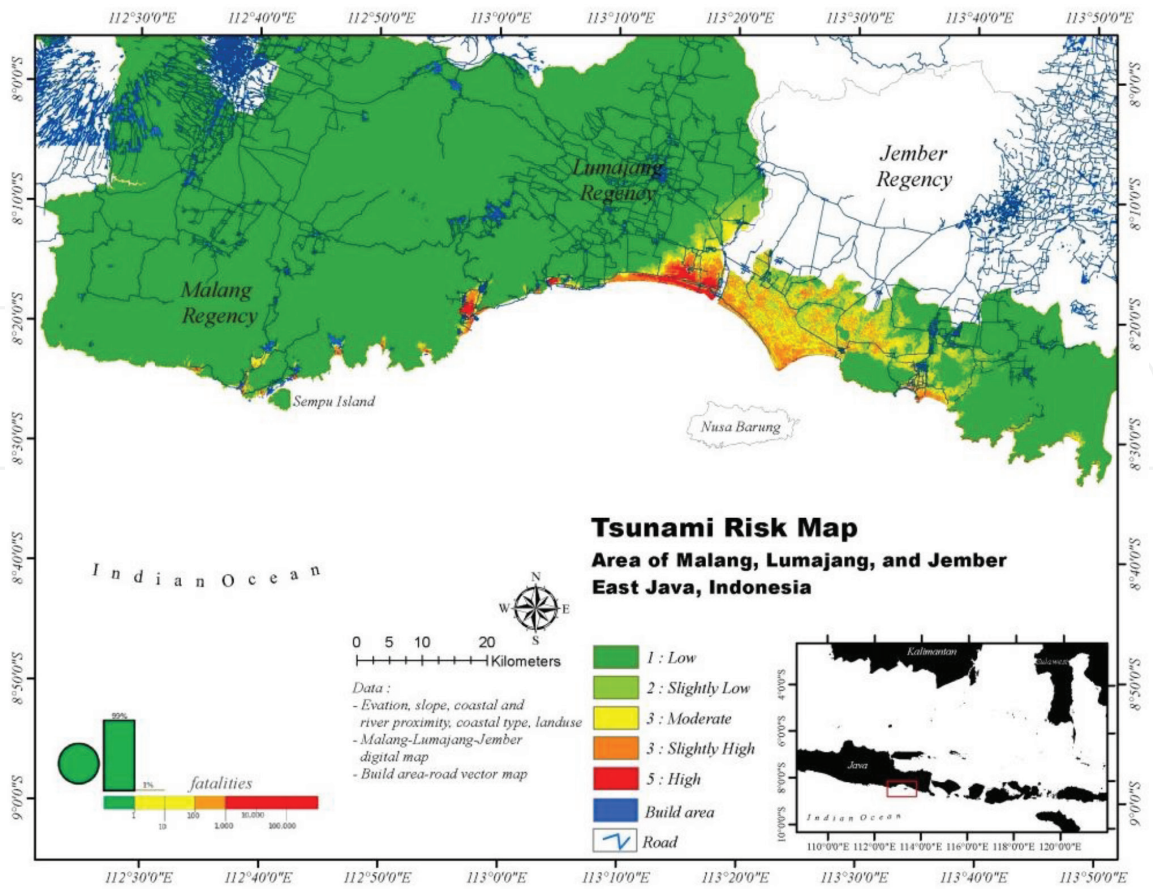

Figure 9.
Tsunami risk map.

out after the 2011 Japan tsunami and found that coastal vegetation is also an important feature to reduce tsunami wave [30]. The high density of mangrove along the coastal area has the capacity to minimize the negative impact of a tsunami wave. Dense mangrove forests growing along coastal areas can help reduce the devastating impact of tsunamis and coastal storms by absorbing some of the wave's energy. When the tsunami struck India's southern state of Tamil Nadu on 26 December, for example, coastal areas with dense mangroves (areas of Pichavaram and Muthupet) suffered fewer human casualties and less damage to property compared to areas without mangroves [40].

The use of pair-wise comparison in AHP process helps in the analysis of spatial multicriteria data where all of the parameters were calculated based on their weight factor. The calculation of weight as a result of pair-wise comparison matrix was created from expert judgment, from a person who was selected based on his/her expertise in tsunami hazard, and disaster mitigation. Tsunami vulnerability research in Alexandria applied all parameters in equal weight due to the limitation of knowledge regarding the study area [14].

High tsunami risk areas were mostly found in the coastal area with the sloping coast type. Elevation and slope play an important role in governing the stability of a terrain. Tsunami vulnerability research in Bali, Indonesia, shows the distribution of vulnerability is not uniform and physically it is highly influenced by coastal proximity, elevation, and slope [29, 37]. Tsunami risk map that described here is based on the integrated approach and provided to the people in the near future due to less information about tsunami risk in the study area.

4. Conclusions

Tsunami risk can be assessed using the application of spatial multicriteria analysis followed by weighted cell-based processing in terms of GIS. DEM data were applied as basic data for creating the parameter of tsunami vulnerability. The result performed here can be used for the evacuation and reconstruction plan due to the tsunami disaster. Also, this will be important basic information in determining both evacuation building and the evacuation route in the coastal areas. Moreover, the final target of tsunami risk mapping is to reduce the effect of the tsunami to the coastal areas where the population is dense by generating a good mitigation plan. The integrated approach of raster weighted overlay of all spatial databases of tsunami vulnerability and risk parameters specified the vulnerability and risk area due to the tsunami and defined the possible area that could be affected by the tsunami and the potential inundated area. The weight of each parameter was calculated by pair-wise comparison matrix from the construction of expert judgment, in which every parameter was weighted not equally.

The overlay processing of tsunami risk map and existing land use, also the distribution of infrastructure and main public facilities, will define the priority area that needs first to be evacuated when tsunami happens. The result of weighted overlay illustrated that high land use of tsunami vulnerability and tsunami risk mostly in the class of urban area in which it is describe the high density of population. Forest area was indicated in the low class of tsunami risk. The green belt mitigation is one of the projects to construct the distribution of coastal vegetation (mangrove) and set it as the barrier zone to reduce the energy of tsunami wave when comes to coastal area and to minimize the negative impact of the wave to the coastal area. More parameters of physical and social vulnerability to tsunami disaster are needed to produce more detailed result.

Acknowledgements

Conflict of interest

The authors declare no conflict of interest.

Author details

Abu Bakar Sambah[1]* and Fusanori Miura[2]

1 Faculty of Fisheries and Marine Science, University of Brawijaya, Malang, Indonesia

2 Environmental Safety Science and Engineering, Graduate School of Science and Engineering, Yamaguchi University, Ube-shi, Japan

*Address all correspondence to: absambah@ub.ac.id

IntechOpen

References

[1] National Geophysical Data Center/ World Data Service (NGDC/WDS). Global Historical Tsunami Database. U.S: National Geophysical Data Center. NOAA; 2014. DOI: 10.7289/V5PN93H7 [Accessed: 4 March, 2014]

[2] Tsunami Generation. Available from: http://pubs.usgs.gov/circ/c1187/

[3] Murata S, Imamura F, Katoh K, Kawata Y, Takahashi S, Takayama T. Tsunami; to Survive from Tsunami. Advanced Series on Ocean Engineering. 2009;**32**:177-239. DOI: 10.1142/7345

[4] Kimura S. Journal of Computer Science. 1987;**1**(2):23-49

[5] Islam MR. Conference proceedings. In: Proceedings of the 2nd International Conference on GEOMATE; 2011. pp. 8-13

[6] UN-ISDR (United Nations International Strategy for Disaster Reduction). 2009. Available from: https://www.unisdr.org/we/inform/terminology

[7] Sambah AB, Miura F, Guntur, Fuad. Integrated satellite remote sensing and geospatial analysis for tsunami risk assessment. International Journal of GEOMATE. 2018;**14**(44):96-101. DOI: 10.21660/2018.44.7127

[8] Sambah AB, Miura F. Spatial data analysis and remote sensing for observing tsunami-inundated areas. International Journal of Remote Sensing. 2016;**37**(9):2047-2065. DOI: 10.1080/01431161.2015.1136450

[9] Karen E, Joyce KC, Wright S, Samsonov V, Ambrosia VG. Remote sensing and the disaster management cycle. In: Jedlovec G, editor. Advances in Geoscience and Remote Sensing. Croatia: InTech; 2009. DOI: 10.5772/8341

[10] Yamazaki F, Kouchi K, Matsuoka M. Tsunami damage detection using moderate-resolution satellite imagery. In: Proceedings of the 8th U.S. National Conference on Earthquake Engineering. San Francisco, CA; 2006. pp. 18-22

[11] Yamazaki F, Matsuoka M. Remote sensing technology in post-disaster damage assessment. Journal of Earthquakes and Tsunamis. World Scientific Publishing Company. 2007;**1**(3):193-210. DOI: 10.1142/S1793431107000122

[12] Carver SJ. Integrating multi-criteria evaluation with geographical information systems. International Journal of Geographical Information Systems. 1991;**5**(3):321-339. DOI: 10.1080/02693799108927858

[13] Jankowski P. Integrating geographical information systems and multiple criteria decision-making methods. International Journal of Geographical Information Systems. 1995;**9**(3):251-273. DOI: 10.1080/02693799508902036

[14] Eckert S, Jelinek R, Zeug G, Krausmann E. Remote sensing-based assessment of tsunami vulnerability and risk in Alexandria, Egypt. Applied Geography. 2012;**32**(2):714-723

[15] Romer H, Willroth P, Kaiser G, Vafeidis AT, Ludwig R, Sterr H, et al. Potential of remote sensing techniques for tsunami hazard and vulnerability analysis—A case study from Phan-Nga province, Thailand. Natural Hazards and Earth System Sciences. 2012;**12**(6):2103-2126

[16] Mahendra RS, Mohanty PC, Bisoyi H, Kumar TS, Nayak S. Assessment and management of coastal multi-hazard vulnerability along the Cuddalore Villupuram, east coast of India using geospatial techniques. Ocean and Coastal Management. 2011;**54**(4):302-311

[17] Strunz G, Post J, Zosseder K, Wegscheider S, Muck M, Riedlinger T, et al. Tsunami risk assessment in Indonesia. Natural Hazards and Earth System Sciences. 2011;**11**(1):67-82

[18] Sinaga TP, Adhi N, Yang-Won L, Yongcheol S. GIS mapping of tsunami vulnerability: Case study of the Jembrana regency in Bali, Indonesia. KSCE Journal of Civil Engineering. 2011;**15**(3):537-543

[19] Gokon H, Koshimura S. Mapping of building damage of the 2011 Tohoku earthquake tsunami in Miyagi prefecture. Coastal Engineering Journal. 2012;**54**(1):126-138

[20] Mori N, Takahashi T, Yasuda T, Yanagisawa H. Survey of 2011 Tohoku earthquake tsunami inundation and run-up. Geophysical Research Letters. 2011;**38**(7):1-6

[21] Dall'Osso F, Bovio L, Cavalletti A, Immordino F, Gonella M, Gabbianelli G. A novel approach (the CRATER method) for assessing tsunami vulnerability at the regional scale using ASTER imagery. Italian Journal of Remote Sensing. 2010;**42**(2):55-74

[22] Maramai A, Tinti S. The 3 June 1994 Java tsunami: A post-event survey of the coastal effects. Natural Hazards. 1997;**15**:31-49

[23] Storchak DA, Di Giacomo D, Bondár I, Engdahl ER, Harris J, Lee WHK, et al. Public release of the ISC-GEM global instrumental earthquake catalogue (1900-2009). Seismological Research Letters. 2013;**84**(5):810-815

[24] Bouvet M, Chander G, Goryl P, Santer R, Saunier S. Preliminary radiometric calibration assessment of ALOS AVNIR-2. In: Geoscience and Remote Sensing Symposium. Barcelona: IGARSS; 2007. pp. 2673-2676

[25] Sah AK, Sah BP, Honji K, Kubo N, Senthil S. Semi-automated cloud/ shadow removal and land cover change detection using satellite imagery. International Archives of the Photogrammetry, Remote Sensing and Spatial Information Sciences. Vol. XXXIX-B7, XXII ISPRS Congress. Melbourne, Australia. 25 August–01 September, 2012. pp. 335-340

[26] Hansen MC, Defries RS, Townshend JRG, Sohlberg R. Global land cover classification at 1km spatial resolution using a classification tree approach. International Journal of Remote Sensing. 2000;**21**:1331-1364. DOI: 10.1080/014311600210209

[27] Han J, Kamper. Data Mining Concept and Techniques. San Francisco, USA: Morgan Kaufmann Publisher; 2011

[28] Friedl MA, Brodley CE. Decision tree classification of land cover from remotely sensed data. Remote Sensing of Environment. 1997;**61**:399-409

[29] Iida K. Magnitude, energy and generation mechanisms of tsunamis and a catalogue of earthquakes associated with tsunamis. In: Proceedings of Tsunami Meeting at the 10th Pacific Science Congress; 1963. pp. 7-18

[30] Van Zuidam RA. Guide to Geomorphologic—Aerial Photographic Interpretation and Mapping. Enschede, The Netherlands: International Institute for Geo-Information Science and Earth Observation; 1983

[31] Sengaji E, Nababan B. Tsunami risk level mapping in Sikka, East Nusa Tenggara. Journal of Tropical Marine Science and Technology. 2009;**1**(1): 48-61 (Indonesia edition)

[32] Smith K. Environmental Hazards-Assessing Risk and Reducing Disaster. 1st ed. London, New York: Routledge; 1992. p. 324

[33] ESRI, Environmental Systems Research Institute, Inc. Analyse Site

Conditions Using Weighted Overlay. New York, USA: ESRI; 2015

[34] Eastman JR, Jin W, Kyem PAK, Toledano J. Raster procedures for multi-criteria/multi-objective decisions, photogrammetric engineering & remote sensing. American Society for Photogrammetry and Remote Sensing. 1995;**61**(5):539-547

[35] Eddy. GIS in disaster management: A case study of tsunami risk mapping in Bali, Indonesia [Masters (Research) Thesis]. Australia: James Cook University; 2006

[36] Niekert D. Introduction to Disaster Risk Reduction. The African Centre for Disaster Studies NWU, Potchefstroom, South Africa: USAID Disaster Risk Reduction Training Course for Southern Africa, Creative Commons Attribution-Share Alike 2.5 South Africa; 2011

[37] Cutter SL, Mitchell JT, Scott MS. Revealing the vulnerability of people and places: A case study of Georgetown country, South Carolina. Annuals of the Association of American Geographers. 2000;**90**:713-737

[38] Papathoma M, Dominey-Howes D. Tsunami vulnerability assessment and its implications for coastal hazard analysis and disaster management planning, Gulf of Corinth, Greece. Natural Hazards and Earth System Sciences. 2003;**3**(6):733-747

[39] Papathoma M, Dominey-Howes D, Zong Y, Smith D. Assessing tsunami vulnerability, an example from Herakleio, Crete. Natural Hazards and Earth System Sciences. 2003;**3**(5):377-389

[40] Zhou H-W. Introduction to seismic data and processing. In: Practical Seismic Data Analysis. Cambridge, United Kingdom: Cambridge University Press; 1991. Available from: http://assets.cambridge.org/97805211/99100/excerpt/9780521199100_excerpt.pdf